Inorg. Chem. **2008**, *47*, 4596−4604

Understanding Selectivity in the Oxidative Addition of the Carbon−Sulfur Bonds of 2-Cyanothiophene to Pt(0)

Tülay A. Ateşin, Abdurrahman Ç. Ateşin, Karlyn Skugrud, and William D. Jones*

Department of Chemistry, University of Rochester, Rochester, New York 14627

Received November 19, 2007

The reaction of 2-cyanothiophene with a zerovalent platinum bisalkylphosphine fragment yields two thiaplatinacycles derived from the cleavage of the substituted and unsubstituted C—S bonds. While cleavage away from the cyano group is preferred kinetically, cleavage adjacent to the cyano group is preferred thermodynamically. Density functional theory using B3LYP level of theory on a model of this system is consistent with experimental results in that the transition state energy leading to the formation of the kinetically favored C—S bond cleavage product is lower by 5.3 kcal mol^{-1} than the barrier leading to the thermodynamically favored product. There is a 6.7 kcal mol^{-1} difference between these two products. The cyano substituent at the 2- position of thiophene did not substantially change the mechanism involved in the C—S bond cleavage of thiophene previously reported.

Introduction

Hydrodesulfurization (HDS) is the industrial process used to remove sulfur-containing compounds from petroleum products. Recent research on HDS has focused on new catalyst design, as today's technologies are insufficient to meet the new regulations on the amount of sulfur allowed in petroleum products.[1] The most commonly used catalyst in industry is a Co−Mo sulfide supported on alumina, although other common combinations include Ni−Mo and Ni−W. Many homogeneous studies of thiophene C−S cleavage have been undertaken to provide a deeper understanding of the initial steps of HDS.[2–7]

As second and third row metals are known to be considerably more active than their first row counterparts,[8] we previously studied the effect of changing the transition metal (Ni, Pd, Pt) on the activation of thiophenic C−S bonds and on the electronic structure of the thiophene metallacycles formed.[9] Both experiment and density functional theory (DFT) show that the thiaplatinacycle formed from oxidative addition of the C—S bond to the platinum fragment is more stable than its nickel and palladium analogs. A detailed understanding of the reactivity of the catalyst is crucial to the optimization of the HDS process. Earlier studies with the rhodium fragment [Cp*Rh(PMe_3)] showed indirect evidence for both η^2-C,C- and S-bound complexes prior to C−H or C−S cleavage.[10] Labeling studies were consistent with the S-bound complex being the immediate precursor to C−S cleavage. In the case of nickel and platinum systems that activated thiophene, no intermediates could be detected, leaving the details of the pathway for C−S cleavage unknown. Another interesting property of the d^{10} 14-electron platinum phosphine fragments is that they can reversibly insert into the C—S bonds of thiophenes. Maitlis and coworkers showed that d^{10} PtL_2 fragments undergo C−S oxidative addition with a variety of thiophenes and phosphine ligands.[11] The density functional calculations on the reaction of parent thiophene with the [Pt(dmpe)] fragment as a model for Pt[(dippe)] were undertaken to probe the mechanism by which thiophene reacts with the metal center.[12] In this detailed study, thiophene binding by σ-complexation of S

* To whom correspondence should be addressed. E-mail: jones@chem.rochester.edu.

(1) Topsøe, H.; Clausen, B. S.; Massoth, F. E. *Hydrotreating Catalysis*; Springer: Berlin, 1996.
(2) Sánchez-Delgado, R. A. *Organometallic Modeling of the Hydrodesulfurization and Hydronitrogenation Reactions*; Kluwer Academic Publishers: Dordrecht, 2002; p 1.
(3) Chen, J.; Daniels, L. M.; Angelici, R. J. *Polyhedron* **1990**, *9*, 1883.
(4) Bianchini, C.; Meli, A.; Peruzzini, M.; Vizza, F.; Frediani, P.; Herrera, V.; Sanchez-Delgado, R. A. *J. Am. Chem. Soc.* **1993**, *115*, 7505.
(5) Garcia, J. J.; Mann, B. E.; Adams, H.; Bailey, N. A.; Maitlis, P. M. *J. Am. Chem. Soc.* **1995**, *117*, 2179.
(6) Luo, S.; Skaugset, A. E.; Rauchfuss, T. B.; Wilson, S. R. *J. Am. Chem. Soc.* **1992**, *114*, 1732.
(7) Li, H.; Carpenter, G. B.; Sweigart, D. A. *Organometallics* **2000**, *19*, 1823.
(8) Ledoux, M. J.; Michaux, O.; Agostini, G.; Panissod, P. *J. Catal.* **1986**, *102*, 275.
(9) Ateşin, T. A.; Oster, S. S.; Skugrud, K.; Jones, W. D. *Inorg. Chim. Acta* **2006**, *359*, 2798.
(10) Dong, L.; Duckett, S. B.; Ohman, K. F.; Jones, W. D. *J. Am. Chem. Soc.* **1992**, *114*, 151.

10.1021/ic702273a CCC: $40.75
Published on Web 05/01/2008

and η^2 π-complexation of C=C were considered as the initial coordination modes of thiophene prior to insertion of the metal into the C—S bond. The solvent effect was also taken into consideration and shown to be of critical importance. Both the ability to insert reversibly into the C—S bonds of thiophenes and the observed regioselectivity has led to the possibility of studying the kinetic and thermodynamic aspects of the C—S bond cleavage process. In this paper, results of kinetic experiments on the reaction of 2-cyanothiophene with the [Pt(dippe)] fragment and DFT calculations using B3LYP level of theory with [Pt(dmpe)] as a model for [Pt(dippe)] to explain the observed selectivities will be presented.

Results and Discussion

Synthesis and Characterization of 3 and 4. Similar to the previous synthesis of [Pt(dippe)(κ^2-S,C-SCH=CHCH=CH)] (**1**),[9] the dinuclear complex [[Pt(dippe)]$_2$(μ-η^2,η^2-COD)] (**2**) was used as a precursor in the synthesis of [Pt(dippe)(κ^2-S,C-SC(CN)=CHCH=CH)] (**3**) and [Pt(dippe)(κ^2-S,C-SCH=CHCH=C(CN))] (**4**) (eq 1). A mixture of C—S bond cleavage products is formed in a 5:1 ratio from the reaction of **2** with 2-cyanothiophene in tetrahydrofuran (THF) at 100 °C after 3 h.

The ^{31}P{^{1}H} NMR spectra of **3** and **4** show two doublets with platinum satellites for each complex arising from two chemically inequivalent phosphine atoms. The phosphine resonances for **3** are at δ 67.17 and 66.86 ($^2J_{P-P}$ = 5 Hz), with $^2J_{Pt-P}$ of 1698 and 3070 Hz, and those for **4** are at δ 65.22 and 65.05 ($^2J_{P-P}$ = 9 Hz), with $^2J_{Pt-P}$ of 1951 and 2909 Hz, respectively. The ^{1}H NMR spectra of both complexes show two multiplets for the methylene resonances of the ethylene linker of the dippe ligand, two multiplets for their methyne protons, and overlapping methyl resonances. The thienyl proton resonances of **3** are at δ 8.649, 7.377, and 7.129, while those for **4** are at δ 7.395, 7.240, and 6.598. In the ^{13}C NMR spectrum of **3**, the carbon resonance at δ 143.0 has coupling to the cis and trans phosphorus of the dippe ligand, ^2J(trans P−C) = 95 Hz, ^2J(cis P−C) = 9 Hz, and platinum satellites, ^1J(Pt−C) = 747 Hz. Because no other carbon resonance has a coupling with platinum as large as this resonance, it was assigned to the carbon directly bound to platinum. The HSQC spectrum of **3** showed a correlation between the carbon resonance at δ 143.0 and the proton resonance at δ 8.649. Therefore, this resonance is assigned to the proton bound to this carbon. Similarly, the proton resonances at δ 7.377 and 7.129 are assigned to the carbon resonances at δ 135.1 and 121.8, respectively. The proton resonances are assigned by using the correlations in the COSY spectrum. The stronger coupling between resonances at δ 8.649 and 7.129 than δ 7.129 and 7.377 indicates a *w*-coupling between the former and a cis-coupling between the latter, allowing assignment of the resonance at δ 7.377 to H2 and 7.129 to H3. These assignments are further ensured by the HMBC spectrum, which indicates that the carbon at δ 135.1 is two or three bonds away from the proton at δ 8.649 (H1) and δ 7.129 (H3). H3 is also shown to be two or three bonds away from the carbon resonance at δ 98.2. Because the carbon at δ 98.2 has platinum satellites, ^1J(Pt−C) = 49 Hz, and it is the only carbon resonance not assigned to a proton resonance; it is assigned to C4. A summary of assignments of the proton and carbon resonances for **3** are listed in Table 1. COSY and HSQC spectra for **3** and **4** are included in the Supporting Information.

Table 1. Assignments of ^{1}H and ^{13}C Resonances in **3**

	Position	Proton	Carbon
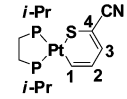	1	8.649	143.0
	2	7.377	135.1
	3	7.129	121.8
	4	-	98.9

The structures of **3** and **4** were also confirmed by a single crystal X-ray structure determination. Crystals of **3** and **4** suitable for X-ray diffraction were grown by slow diffusion of pentane into a THF solution. POV-RAY drawings of their molecular structures are shown in Figure 1, and selected bond lengths and angles are shown in Table 2, while crystallographic data for both complexes are summarized in Supporting Information, Table SI-1. Notable features of the molecular structures of **3** and **4** are the square-planar geometries around the metal center, the planar thienyl ligand, and the clear bond-length alternation (short–long–short) within the thiophenic ring. These bond lengths are consistent with those reported for the substituted thiaplatinacycles in the literature.[11]

Kinetic Results. A slow exchange reaction occurs between **1** and 2-cyanothiophene at 160 °C, and can easily be followed

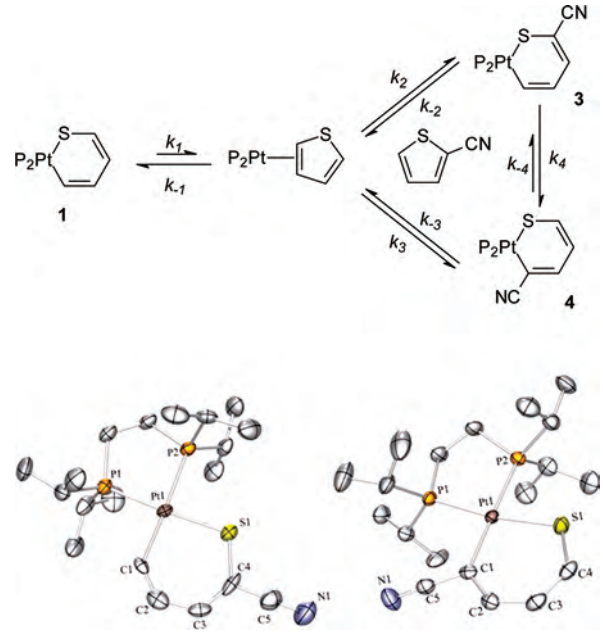

Figure 1. POV-RAY images of the molecular structures of **3** and **4** showing the labeling of the atoms around the Pt atom. Displacement ellipsoids are drawn at the 50% level. Hydrogens have been removed for clarity.

(11) (a) Garcia, J. J.; Arevalo, A.; Capella, S.; Chehata, A.; Hernandez, M.; Montiel, V.; Picazo, G.; Del Rio, F.; Toscano, R. A.; Adams, H.; Maitlis, P. M. *Polyhedron* **1997**, *16*, 3185. (b) Garcia, J. J.; Arevalo, A.; Montiel, V.; Del Rio, F.; Quiroz, B.; Adams, H.; Maitlis, P. M. *Organometallics* **1997**, *16*, 3216.

(12) Ateşin, T. A.; Jones, W. D. *Organometallics* **2008**, *27*, 53–60.

Table 2. Selected Bond Lengths and Angles for **3** and **4**

	3	4		3	4
			Selected Bond Lengths (Å)		
Pt—C(1)	2.064(7)	2.071(4)	N—C(5)	1.190(11)	1.166(5)
C(1)—C(2)	1.261(10)	1.368(5)	S—C(4)	1.743(9)	1.694(4)
C(2)—C(3)	1.412(11)	1.419(6)	Pt—S	2.280(2)	2.2984(11)
C(3)—C(4)	1.366(12)	1.358(6)	Pt—P(1)	2.2591(19)	2.2866(11)
C(4/1)—C(5)	1.410(12)	1.403(6)	Pt—P(2)	2.3112(19)	2.3051(10)
			Selected Angles (°)		
C(1)—Pt—P(1)	92.5(2)	95.00(12)	C(1)—Pt—S	92.4(2)	92.82(12)
P(1)—Pt—S	172.69(8)	171.56(4)	C(5)—C(4)—S	112.9(7)	
C(1)—Pt—P(2)	174.10(18)	177.90(12)	C(5)—C(1)—Pt		121.2(3)
S—Pt—P(2)	89.22(7)	85.74(4)	N—C(5)—C(4/1)	178.7(11)	178.4(5)

by ^{31}P NMR spectroscopy, as shown in Figure 2. The kinetic oxidative addition product **3** predominates initially, forming in a ratio to **4** of >5:1. This ratio corresponds to a $\Delta\Delta G^{\ddagger}_{433}$ of >1.4 kcal/mol for the two C—S bond cleavage pathways. Over a period of days, the ratio of **3**:**4** reaches an equilibrium ratio of 2:98 corresponding to a ΔG_{433} of −3.4 kcal/mol. Because the synthesis of the C—S bond cleavage products of 2-cyanothiophene from its reaction with **2** requires a lower temperature (100 °C) and consumes **2** within a couple of hours (eq 1), the rate limiting step in the exchange reaction with **1** was expected to be the dissociation of thiophene from **1**. However, evidence for an associative mechanism was observed as described below.

The decay of **1** was followed as a function of increasing concentrations of 2-cyanothiophene. The disappearance of **1** follows a first order rate law under these pseudo first order conditions (Figure 3). As the concentration of 2-cyanothiophene was increased from 0.25 M (10 equiv with respect to **1**) to 0.51 M (20 equiv) and 1.02 M (40 equiv), the rate of the decay of **1** also increased, suggesting an associative mechanism. However, the dependence of the pseudo first order rate constant k_{obs} on the concentration of 2-cyanothiophene was not linear but showed downward curvature (Figure 4, inset). This dependence could be explained, however, in terms of a reversible thiophene elimination to generate an intermediate π-complex followed by a rate determining reaction with 2-cyanothiophene (eq 2). For such a mechanism, a plot of $1/k_{obs}$ versus 1/[2CNTP] should be linear, with an intercept of $1/k_1$ and a slope of k_{-1}/k_1k_{23} (see Supporting Information). This plot is shown in Figure 4, and provides values of $k_1 = 1.6(1) \times 10^{-5}$ s^{-1} and $k_{-1}/k_{23} = 0.35(3)$ M^{-1}.

In a separate experiment, 10 equiv each of thiophene and 2-cyanothiophene were added to a THF solution of **2** at 100 °C. Formation of **3** and **4** were observed as the sole products when the reaction was followed by ^{31}P NMR spectroscopy, indicating that back reaction of the free [Pt(dippe)] fragment with thiophene is slow compared to reaction with 2-cyanothiophene. Together, these experiments provide strong evidence for an associative mechanism for the exchange of thiophene in **1**.

While **3** was observed as the favored kinetic product of the reaction, over time **4** is formed as the major product. Kinetic data for the distribution of species were collected at 160 °C over several days. Simulations for the associative pathway were carried out using the KINSIM/FITSIM programs to obtain best fit rate constants for the overall process given in Scheme 1.[13] In the simulation, the values of k_1, k_2, k_3, and k_4 were allowed to vary freely. The value for k_{-1} was linked to $k_2 + k_3$ ($= k_{23}$) based upon the double reciprocal analysis (see Supporting Information for details). On the basis of the position of the final equilibrium, k_{-4} was set to $k_4/49$. The reverse rate constants k_{-2} and k_{-3} were set to zero based on the observation that no **1** remains at the end of the reaction. The calculated rate constants for this process are given in Table 3, while the fits of concentration versus time are shown by the solid lines in

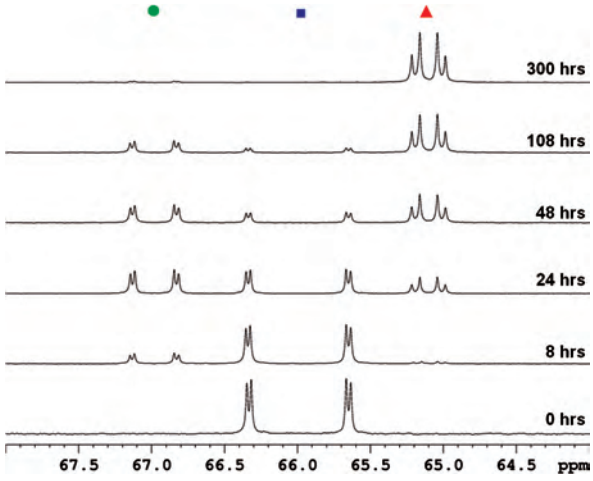

Figure 2. ^{31}P NMR spectra (400 MHz) illustrating the change in the concentration of the species involved in the reaction of PtT (26 mM) with 20 equiv of 2-cyanothiophene (520 mM) in THF at 160 °C as a function of time. (●, **3**; ■, **1**; ▲, **4**). Pt satellites not shown.

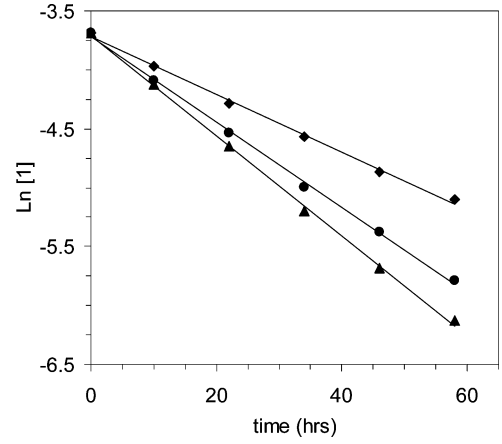

Figure 3. Logarithmic change in concentration of **1** as a function of reaction time at different concentrations of 2-cyanothiophene (0.25 M, ◆; 0.51 M, ●; 1.02 M, ▲). The solid line reflects the best fit based on linear regression.

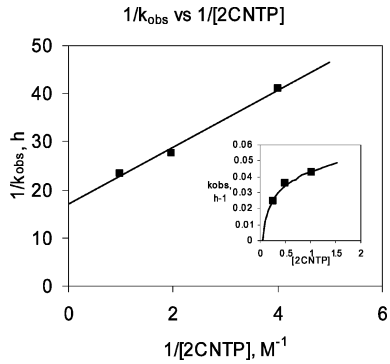

Figure 4. Double reciprocal plot for the rate constants from Figure 3. The inset shows the direct plot of k_{obs} vs [2CNTP].

Scheme 1. Associative Mechanism

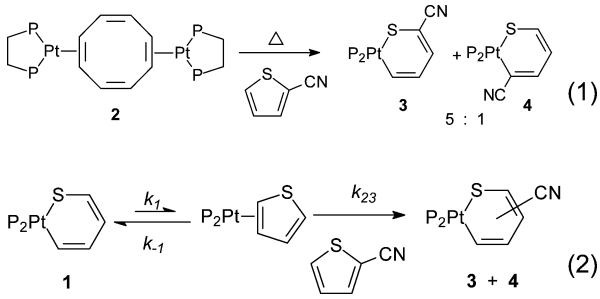

Table 3. Summary of Simulated Rate Constants for the Reaction of **1** with 2-Cyanothiophene at 160 °C[a]

rate constant	k	rate constant	k, h^{-1}
k_1	$7.79\ (5) \times 10^{-4}\ s^{-1}$	k_3	$6.6\ (75) \times 10^{-4}\ M^{-1}\ s^{-1}$
k_{-1}	$2.1\ (10) \times 10^{-2}\ s^{-1}$	k_4	$4.74\ (8) \times 10^{-6}\ s^{-1}$
k_2	$6\ (3) \times 10^{-2}\ M^{-1}\ s^{-1}$	k_{-4}	$9.7\ (2) \times 10^{-6}\ s^{-1}$

[a] k_{-2} and k_{-3} were set to 0. The ratio of k_4/k_{-4} was set to 49 from the final equilibrium position, and the ratio of k_{-1}/k_2 was set to 0.347 from the double reciprocal plot. All other rate constants were allowed to vary independently. Errors are indicated in parenthesis.

Figure 5. Note that $k_3 \ll k_2$, implying that the kinetic product **3** is formed 92 × faster than the thermodynamic product **4**.

Computational Results. DFT calculations havebeen used to investigate the observed kinetic and thermodynamic selectivities observed in these bond cleavage reactions. To simplify the calculations, the *i*-Pr groups in the [Pt(dippe)] fragment were substituted by methyl groups. Calculations with the four isopropyl groups are not only much more computationally demanding but also were found to oscillate between several rotational minima of the isopropyl groups, slowing convergence without providing any real new important insights into the understanding of the intermediates/processes involved. This substitution is assumed to have no steric outcome on the calculations, as the single crystal X-ray structures showed no interaction between the methyl groups of the dippe ligand and the thiophene ring.[9] We did not explore the use of the Pt(dmpe) fragment experimentally, as it is known to form $Pt(dmpe)_2$ upon heating.[14]

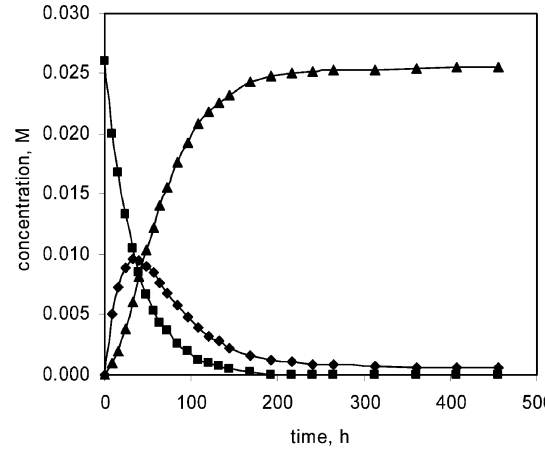

Figure 5. Change in concentration of **1** (■), **3** (◆), and **4** (▲) during the reaction of 26 mM **1** with 20 equiv of 2-cyanothiophene (520 mM) in THF as a function of time. The solid line reflects the simulated data.

The experimental structures for the oxidative addition products, whose POV-RAY images are shown in Figure 1, were used as the starting point for all of the calculations. The optimization of all of the ground-state and the transition state structures was done in the gas phase. The optimized structures of the stationary points on the potential energy surface for cleavage of the substituted and unsubstituted C—S bonds of 2-cyanothiophene are shown in Figures 6 and 7, respectively. The structural parameters for all structures as well as the energetics relative to the free fragments are given in Table 4. The energies in gas phase are the Gibbs free energies calculated at 298 K, and those calculated with the polarized continuum model (PCM) correction are the total free energies in solution.

As we have found with the parent thiophene system,[12] there are three stable species: one with an η^2-C,C-thiophene, one with an η^2-C,S-thiophene, and one with an S-bound thiophene. Because of the presence of the cyano group, however, there are now two distinct η^2-C,C- and η^2-C,S-thiophene complexes. The η^2-C,C- species has been found to interconvert with the η^2-C,S- species, which in turn interconverts with the S-bound species. The η^2-C,S- species is also the immediate precursor of the C−S cleavage product. Neither the η^2-C,C- nor S-bound thiophene complexes go directly to the oxidative addition product. A description of these stable species and the transition states connecting them provides a continuous picture of the bond making/bond breaking processes.

The carbon atom in the C—S bond being broken is numbered as C1 in all structures (see Figure 1 for numbering). In the η^2-C,C-complexes **S1** and **S1′**, 2-cyanothiophene binds to the metal center through its substituted and unsubstituted π bonds, respectively, between the C1 and *C*2 atoms in an η^2 fashion. The Pt—C1 and Pt—C2 distances are short, around 2.11 and 2.15 Å, and the Pt—S distances are long

(13) (a) Barshop, B. A.; Wrenn, R. F.; Frieden, C. *Anal. Biochem.* **1983**, *130*, 134–145. (b) Zimmerle, C. T.; Frieden, C. *Biochem. J.* **1989**, *258*, 381–387.

(14) Nuzzo, R. G.; McCarthy, T. J.; Whitesides, G. M. *Inorg. Chem.* **1981**, *20*, 1312.

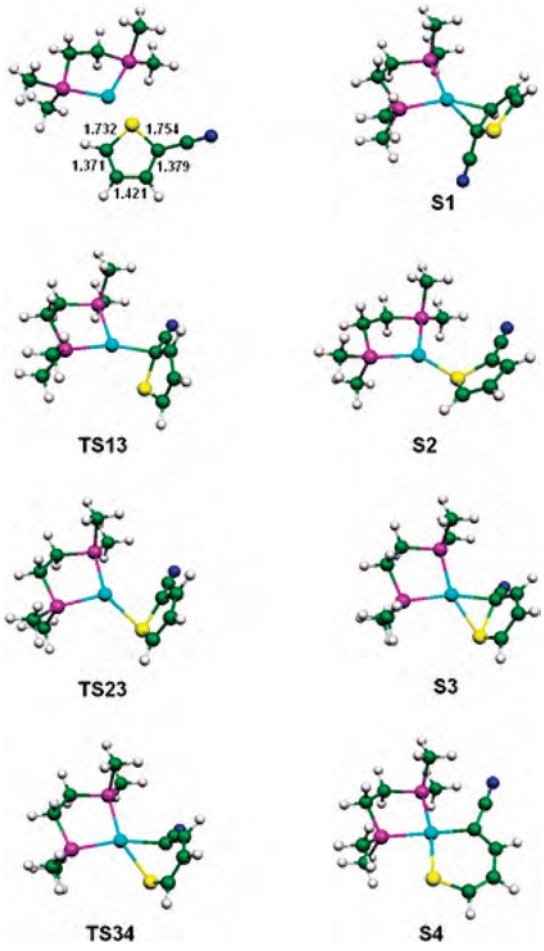

Figure 6. Gas phase optimized structures of stationary points on the potential energy surface of the substituted C—S bond cleavage.

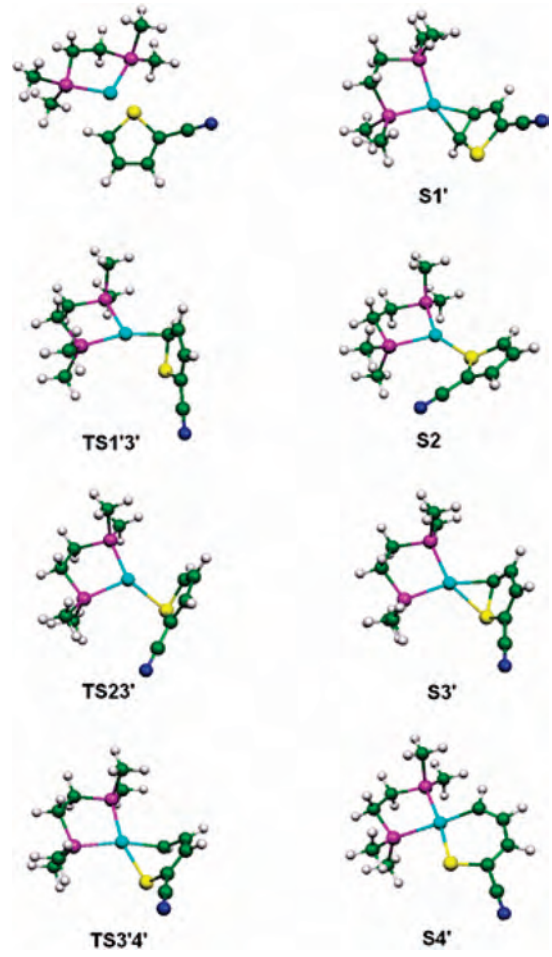

Figure 7. Gas phase optimized structures of stationary points on the potential energy surface of the unsubstituted C—S bond cleavage.

(∼ 3.40 Å). Both C1 and C2 show a decrease in their sp^2 hybridization to become more like sp^3 hybridized carbons. The C1—C2 bond lengths (∼1.47 Å) are consistent with a C—C single bond and the S—C1 bonds are slightly lengthened (∼1.82 Å) from ∼1.74 Å in free 2-cyanothiophene. The bound thiophene molecules are at an angle of 113.6° and 111.4° to the P—Pt—P plane in **S1** and **S1′**, respectively.

Starting with the stable olefin complexes, **S1** and **S1′**, the Pt—S distances (∼2.69 Å) are dramatically shortened to reach transition states **TS13** and **TS1′3′** for migration to the η^2-C,S-complexes. The 2-cyanothiophene molecules are tilted because of their rotation around the Pt—C1 axis to bring the sulfur atom closer to the Pt atom. The Pt—C2 bond lengths are substantially longer (2.873 and 2.716 Å).

The η^1 character of S-bound thiophene complex **S2** is clear from the short Pt—S distance of 2.295 Å and the two long Pt—C1 and Pt—C4 distances of about 3.57 Å. The η^1 coordination does not affect the π system of the thiophene, and the S—C1 and S—C4 bond lengths before and after binding are nearly the same. The bound 2-cyanothiophene molecule is at an angle of 147.5° to the P—Pt—P plane.

Transition states **TS23** and **TS2′3′** for migration from the S-bound to the η^2-C,S-thiophene complexes result from the rotation of 2-cyanothiophene in its molecular plane in **S2** to reduce the Pt—C1 distance to form the Pt—C1 bond. The C1—S—C4 planes are at angles of about 118.7° and 111.0°, respectively, to the P—Pt—P planes. The C1 atoms show evidence of possessing partial sp^3 character. The S—C1 bond lengths (∼1.76 Å) are not so different from their values in the initial complex **S2** (1.779 Å) and the Pt—C1 and Pt—S bond lengths (∼2.77 and ∼2.44 Å, respectively) are closer to their value in the η^2-C,S coordinated complexes **S3** and **S3′** (∼2.17 and 2.47 Å). The C1—C2, C2—C3, and C3—C4 bond lengths (∼1.39, ∼1.41, and ∼1.38 Å) are between a C—C single and C═C double bond, indicating extensive electron delocalization between these atoms.

In the η^2-C,S-coordinated complexes **S3** and **S3′**, 2-cyanothiophene binds to the metal center through its substituted and unsubstituted C1—S bonds, respectively. Although a greater lengthening is observed in the substituted C1—S bond (1.873 Å) in **S3** than that for the unsubstituted one (1.827 Å) in **S3′**, both have similar Pt—C1 and Pt—S distances around 2.17 and 2.47 Å. Furthermore, the C1 atoms have lost much of their sp^2 hybridization to take on more sp^3 character. The bound thiophene molecules are at angles of 116.5° and 112.3°, respectively, to the P—Pt—P planes. The π systems are involved in the bonding, as the S—C1, C1—C2, C2—C3, and C3—C4 bond lengths are different in comparison with those in free 2-cyanothiophene. The C1—C2 bond lengths (∼1.44 Å) are closer to a C—C single bond, whereas the C2—C3 and

Table 4. Gas Phase Optimized Structures (Interatomic Distances in Å) and Relative Gibbs Free Energies (ΔG/kcal mol^{-1}) of Stationary Points in Schemes **3** and **4**[a]

	Pt—S	Pt—C1	Pt—C2	S—C1	C1—C2	C2—C3	C3—C4	C4—S	C4—C5	ΔG[b]	ΔG[c]	μ[d]
S1	3.405	2.122	2.140	1.831	1.477	1.466	1.349	1.767	1.432	−17.90	−22.73	10.76
S1′	3.367	2.109	2.160	1.817	1.464	1.453	1.363	1.784	1.416	−17.95	−22.51	9.48
TS13	2.667	2.139	2.873	1.832	1.443	1.406	1.379	1.737	1.435	−1.04	−3.60	10.50
TS1′3′	2.717	2.114	2.716	1.807	1.441	1.402	1.391	1.765	1.406	−4.94	−8.89	7.42
S2	2.295	3.564	4.623	1.779	1.375	1.426	1.368	1.747	1.413	−7.21	−8.47	4.64
TS23	2.466	2.745	3.662	1.780	1.397	1.413	1.376	1.744	1.419	1.83	0.70	7.45
TS23′	2.422	2.807	3.681	1.749	1.391	1.408	1.390	1.771	1.407	−1.99	−2.30	6.25
S3	2.479	2.183	3.137	1.873	1.440	1.393	1.390	1.730	1.434	−3.32	−5.30	11.79
S3′	2.458	2.167	3.120	1.827	1.444	1.380	1.412	1.759	1.402	−8.22	−13.59	8.38
TS34	2.423	2.153	3.151	1.977	1.429	1.396	1.387	1.732	1.432	−2.57	−5.66	12.58
TS3′4′	2.376	2.089	3.120	2.144	1.408	1.398	1.394	1.767	1.411	−4.35	−10.92	8.91
S4	2.345	2.060	3.113	3.211	1.377	1.429	1.361	1.726	1.425	−40.08	−52.38	14.01
S4′	2.333	2.022	3.078	3.204	1.365	1.433	1.368	1.752	1.431	−32.85	−45.63	8.88

[a] Atom numbering is as shown in Figure 1. [b] Gibbs free energies in gas phase. [c] Total free energies in THF solution. [d] Dipole moment in Debye.

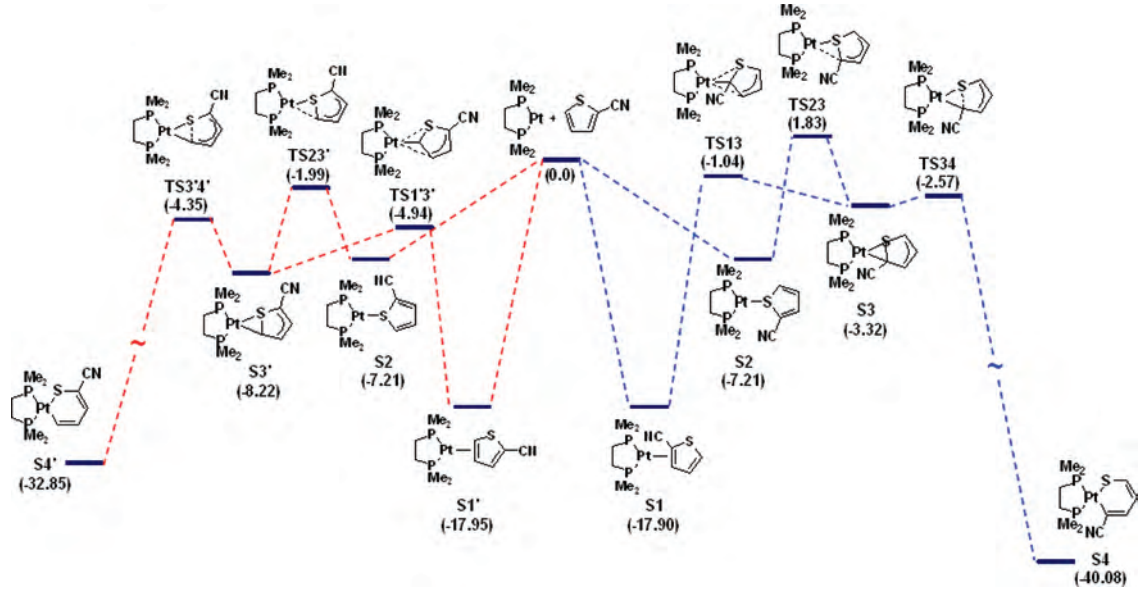

Figure 8. Energetics of the cleavage of the C—S bonds of 2-cyanothiophene by [Pt(dmpe)] in gas phase (kcal mol^{-1}).

C3—C4 bonds (∼1.39 and ∼1.40 Å) are in between a C—C single bond and *C*═C double bond, indicating electron delocalization between *C*2, C3, and C4.

The S—C1 bond lengths in **TS34** and **TS3′4′** for the oxidative cleavage are significantly different from each other. The one in **TS34** (1.977 Å) is only about 0.1 Å longer than its value in the initial complex **S3**, whereas the one in **TS3′4′** (2.144 Å) is 0.3 Å longer. The Pt—C1 and Pt—S bond lengths in **TS34** (2.153 Å and 2.423 Å) are also closer to their values in the initial complex **S3**, while those for **TS3′4′** (2.089 Å and 2.376 Å) are closer to their values in the oxidative addition product **S4′** and only 0.04 and 0.07 Å shorter from their final values. In **TS34**, the C1—C2 bond length (1.429 Å) is closer to a C—C single bond, whereas the C2—C3 and C3—C4 bonds are between a C—C single bond and a C═C double bond, indicating electron delocalization between the C2, C3, and C4 atoms. In contrast, the electron delocalization in **TS3′4′** is extended to all carbon atoms in the thiophenic ring. Consequently, **TS3′4′**, which leads to the kinetic product, appears to be further along the reaction coordinate toward C−S cleavage. This result was unexpected, in that the presence of an α-cyano group in **TS34** was expected to result in greater stabilization of a ring-opened product because of the carbenoid nature that C1 takes on, thereby rendering this transition state further along the reaction coordinate.

In the oxidative addition products **S4** and **S4′**, the metal has inserted between the C1 and the S atoms to form the square planar complexes. The six-membered rings adopt a planar geometry and have clear bond-length alternation (short–long–short) within the thiophenic rings. In all of the transition state structures described above, the C2—C3 bonds are considerably shorter while the C3—C4 bonds are considerably longer than those in free 2-cyanothiophene; therefore a delocalization of electron density between the C2, C3, and C4 atoms is shown in the figures representing these transition states.

Effect of Solvation. The relative energies of the optimized structures were calculated with respect to the total energies of the free fragments. Figure 8 demonstrates the Gibbs free energies calculated *in the gas phase* for the cleavage of the C—S bonds of 2-cyanothiophene by [Pt(dmpe)] in kcal mol^{-1}. The cleavage of the substituted C—S bond is shown on the right-hand side with blue dashed lines, and that of the unsubstituted one on the left with red dashed lines. As the cyano substituent is a very polar group, the effect of

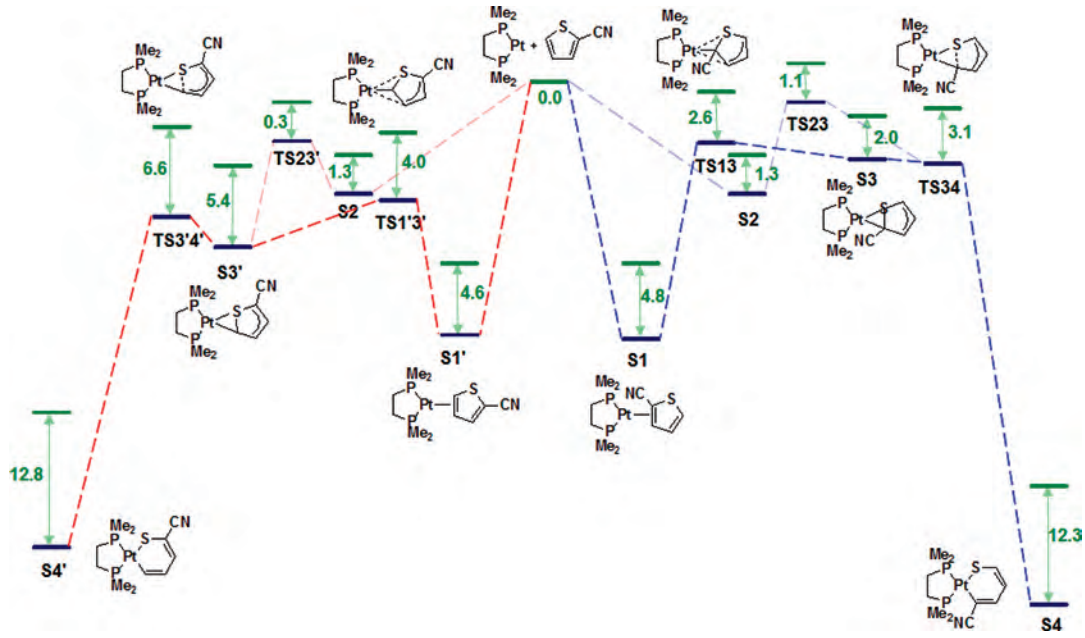

Figure 9. Change in the energetics of the cleavage of C—S bonds of 2-cyanothiophene by [Pt(dmpe)] after PCM corrections (kcal mol^{-1}).

solvation on the energies of these species was also examined. In Figure 9, green data points represent the gas phase energies shown in Figure 8, and the dark blue data points represent the total free energies in solution after solvation in THF is taken into account using the polarizable continuum model (PCM) corrections. The color code for the dashed lines is the same as in Figure 8.

In THF solution, the relative energies of the C═C double bond coordinated complexes as well as the transition states arising from them are significantly lower than their S-coordinated counterparts. Gas phase calculations also show that the transition state **TS23** is higher in energy than the total energy of the free fragments, indicating dissociation of 2-cyanothiophene from [Pt(dmpe)] during the migration of the metal atom from the S atom to the substituted C—S bond. However, when solvation in THF is taken into account the energetics change significantly. Because of the large polarity differences in the platinum-thiophene complexes (see Table 4), the different species are stabilized by THF to different extents. Among the ground-state structures, the polar oxidative addition products, **S4** and **S4′**, were stabilized the most (∼13 kcal mol^{-1}), the C═C double bond coordinated thiophene complexes, **S1** and **S1′**, were stabilized to a lesser extent (∼5 kcal mol^{-1}), and the S-coordinated thiophene complex, **S2**, was stabilized the least (∼1 kcal mol^{-1}) as it is the least polar species. Likewise, the transition states leading to the oxidative addition products, **TS34** and **TS3′4′**, were stabilized more (3–7 kcal mol^{-1}) than the transition state structures **TS13** or **TS1′3′** (3–4 kcal mol^{-1}), while those arising from the S-coordinated thiophene **TS23** and **TS23′** were the least stabilized (∼1 kcal mol^{-1}). In fact, the transition state for the cyano substituted C—S bond cleavage, **TS34**, is now lower in energy than the ground-state energy of the η^2-C,S coordinated thiophene, **S3**, which in turn is lower in energy than **TS13**. Therefore, the C═C double bond coordinated intermediate, **S1**, connects via **TS13** directly to the oxidative addition product **S4**. On the unsubstituted side, the transition state from the C═C double bond coordinated intermediate, **TS1′3′**, is below the ground-state energy of the S-coordinated thiophene, **S2**, and connects to the η^2-C,S coordinated thiophene, **S3′**, which then goes on to the cleavage product via a lower barrier in **TS3′4′**.

On the basis of the DFT results, similar to the parent thiophene system,[12] the reaction of 2-cyanothiophene with the [Pt(dippe)] fragment also proceeds via initial coordination of 2-cyanothiophene through the C═C double bonds. These adducts are sufficiently weakly bound (∼22 kcal mol^{-1}) that they would readily interchange under the reaction conditions. In the gas phase calculations, migration of the metal toward the S atom of the 2-cyanothiophene leads to the formation of the higher energy η^2-C,S coordinated thiophenes, **S3** and **S3′**, and the oxidative addition takes place through these intermediates. On the other hand in THF, the η^2-C,S coordinated thiophene, **S3**, is no longer a stable intermediate between the C═C double bond coordinated thiophene and the oxidative addition product. Note that in agreement with experiment, the transition state leading to the kinetic product **S4′** is still lower than the barrier for formation of the thermodynamic isomer **S4**, with the energy difference between them increased to 5.3 kcal mol^{-1} from 3.3 kcal mol^{-1} in the gas phase. In addition, the oxidative addition product **S4** is substantially preferred over **S4′**, also in agreement with experiment. Because all of the transition state energies are found to be below the total energy of the free fragments, isomerization can take place without dissociation of 2-cyanothiophene from the [Pt(dippe)] fragment, but under the reaction conditions used to render **1** labile, the η^2-C,C-complexes would also be labile.

Conclusions

Reaction of 2-cyanothiophene with the [Pt(dippe)] fragment yields a kinetic and a thermodynamic thiaplatinacycle

derived from cleavage of the unsubstituted and substituted C—S bonds, respectively. DFT calculations (including solvation effects) gave an energy difference of 5.3 kcal mol^{-1} between the transition states leading to the formation of the kinetically and thermodynamically favored C—S bond cleavage products. Moreover, in the transition state involved with the kinetic product, there exists a greater extent of delocalization, and it appears to be further along the reaction coordinate toward C—S cleavage. There is a 6.7 kcal mol^{-1} energy difference in the opposite direction between these two products. Although the cyano substituent at the 2-position of thiophene did not substantially change the mechanism involved in the C—S bond cleavage of thiophene reported previously,[12] the cascade for the C—S bond cleavage reactions are found to be simplified after PCM solvation corrections. Especially in the case of the cleavage of the substituted C—S bond, the η^2-C,C complex is now directly connected to the C—S bond cleavage product without a stable η^2-C,S intermediate. The barrier for thiophene dissociation is much too high ($\Delta G^{\ddagger} = 45.6$ kcal mol^{-1}) for dissociative substitution consistent with kinetic measurements indicating associative thiophene substitution.

Experimental Section

General Procedures and Materials. Unless otherwise stated, all reactions and manipulations were carried out in dry glassware using standard Schlenk and glovebox techniques, under an inert atmosphere. Solvents were dried and distilled before use from dark purple solutions of sodium/benzophenone ketyl. Also, deuterated solvents (Cambridge Isotope Laboratories) for NMR experiments were dried over sodium/benzophenone ketyl and distilled under vacuum. 2-Cyanothiophene (99%) was purchased from Aldrich Chemical Co., Inc. All other reagent grade chemicals, filter aids, as well as the chromatographic materials were used without any further purification. All NMR spectra were recorded on a Bruker Avance 400 MHz spectrometer in acetone-d_6 or THF-d_8 unless otherwise stated. ^{1}H chemical shifts (δ in ppm) are relative to the deuterated solvent residual protons, and ^{31}P NMR chemical shifts (δ in ppm) are relative to an external 85% solution of H_3PO_4 in the appropriate solvent. Desert Analytics, Inc. carried out all elemental analyses. The synthesis of [Pt(dippe)]$_2$(μ-η^2,η^2-COD)] was carried out using the reported procedure.[15] All complexes were purified by crystallization.

Synthesis of C−S Insertion Products 3 and 4. [Pt(dippe)]$_2$(μ-η^2,η^2-COD)] (26.3 mg, 0.051 mmol) was dissolved in 0.6 mL of THF and transferred to a resealable NMR tube. 2-Cyanothiophene (24 μL, 0.255 mmol) was added, and the contents of the tube were heated at 100 °C for 3 h. The solvent, excess 2-cyanothiophene, and COD were evaporated under vacuum to yield 22.7 mg of a yellow solid (81%). Anal. Calcd for a 2.7:1.0 mixture of **3** and **4**, $C_{19}H_{35}NP_2PtS$: C 40.28, H 6.23, N 2.47. Found: C 40.65, H 6.40, N 2.49. For **3**, ^{1}H NMR (400 MHz, acetone-d_6, 25 °C): δ 8.649 (m, 1H), 7.377 (d, $J_{P-H} = 7.9$ Hz, 1H), 7.129 (m, 1H), 2.655 (m, 2H), 2.448 (m, 2H), 2.204 (m, 2H), 2.008 (m, 2H), 1.344–1.152 (m, 24H). ^{13}C{^{1}H} NMR (100 MHz, acetone-d_6, 25 °C): δ 143.0 (d, $J_{P-C} = 95$ Hz, $J_{P-C} = 9$ Hz, $J_{Pt-C} = 747$ Hz), 136.3 ($J_{Pt-C} = 21$ Hz), 135.1 ($J_{Pt-C} = 117$ Hz), 121.8 (s), 98.2 (s, $J_{Pt-C} = 49$ Hz), 24.8 (d, $J_{P-C} = 27$ Hz), 23.7 (d, $J_{P-C} = 32$ Hz), 20.6 (d, $J_{P-C} = 8$ Hz), 20.4 (d, $J_{P-C} = 7$ Hz), 18.2 (d, $J_{P-C} = 34$ Hz), 17.4 (d, $J_{P-C} = 32$ Hz). ^{31}P{^{1}H} NMR (162 MHz, THF-d_8, 25 °C): δ 67.17 (d, $J_{P-P} = 4.9$ Hz, $J_{Pt-P} = 1698.3$ Hz), 66.86 (d, $J_{P-P} = 4.9$ Hz, $J_{Pt-P} = 3070.2$ Hz). For **4**, ^{1}H NMR (400 MHz, THF-d_8, 25 °C): δ 7.395 (m, 1H), 7.240 (s, 1H), 6.598 (m, 1H), 3.314 (m, 2H), 2.461 (m, 2H), 1.997 (m, 2H), 1.764 (m, 2H), 1.229–1.055 (m, 24H). ^{13}C{^{1}H} NMR (100 MHz, THF-d_8, 25 °C): δ 133.9 (s, $J_{Pt-C} = 19$ Hz), 126.1 (s), 126.0 (s), 122.4 (d, $J_{P-C} = 6$ Hz), 120.8 (s, $J_{Pt-C} = 117$ Hz), 21.2 (s, $J_{P-C} = 27$ Hz), 19.3 (d, $J_{P-C} = 5$ Hz), 18.2 (d, $J_{P-C} = 9$ Hz), 17.9 (d, $J_{P-C} = 9$ Hz), 16.0 (d, $J_{P-C} = 73$ Hz), 15.6 (d, $J_{P-C} = 7$ Hz). ^{31}P{^{1}H} NMR (162 MHz, THF-d_8, 25 °C): δ 65.22 (d, $J_{P-P} = 8.9$ Hz, $J_{Pt-P} = 1951.2$ Hz), 65.05 (d, $J_{P-P} = 8.9$ Hz, $J_{Pt-P} = 2909.3$ Hz).

Kinetics of Reaction of Pt(dippe)(κ^2-S,C-SC_4H_4), 1, with 2-Cyanothiophene. Pt(dippe)(κ^2-S,C-SC_4H_4) (8.9 mg, 0.016 mmol) was dissolved in 0.6 mL of THF and transferred to a sealable NMR tube. 2-Cyanothiophene (31 μL, 0.33 mmol) was then added and the contents of the NMR tube were freeze-pumped-thawed three times before sealing the NMR tube under partial nitrogen pressure. The NMR tube was placed in a steel tube in a GC oven at 160 °C, and the reaction was monitored periodically by inverse gated ^{31}P{^{1}H} NMR spectroscopy.

Caution! *This temperature is well above the solvent boiling point and an explosion hazard is present while the samples are hot.*

Computational Details. The experimentally determined structures of the complexes were used as the starting point for the calculations. To simplify these calculations, the *i*-Pr groups were substituted by methyl groups. This simplification is assumed to have no steric outcome on the calculations but may underestimate the donating ability of the P_2Pt fragment. The gas phase structures were fully optimized in redundant internal coordinates[16] with the DFT and a wave function incorporating Becke's three-parameter hybrid functional (B3),[17] along with the Lee–Yang–Parr correlation functional (LYP).[18] Previous studies of the parent thiophene system demonstrated this to be a suitable functional.[12] All calculations were performed using the Gaussian03[19] package. The Pt, P, and S atoms were represented with the effective core pseudopotentials of the Stuttgart group, and the associated basis sets were improved with a set of f-polarization functions for Pt ($\alpha = 0.993$)[20] and a set of d-polarization functions for P ($\alpha = 0.387$) and S ($\alpha = 0.503$).[21] The remaining atoms (C, H, and N) were represented with

(15) Schager, F.; Haack, K. J.; Mynott, R.; Rufińska, A.; Pörschke, K. R. *Organometallics* **1998**, *17*, 807.

(16) Peng, C.; Ayala, P. Y.; Schlegel, H. B.; Frisch, M. J. *J. Comput. Chem.* **1996**, *17*, 49.

(17) Becke, A. D. *J. Chem. Phys.* **1993**, *98*, 5648.

(18) Lee, C.; Yang, W.; Parr, R. G. *Phys. Rev. B* **1988**, *37*, 785.

(19) Frisch, M. J.; Trucks, G. W.; Schlegel, H. B.; Scuseria, G. E.; Robb, M. A.; Cheeseman, J. R.; Montgomery, J. A., Jr.; Vreven, T.; Kudin, K. N.; Burant, J. C.; Millam, J. M.; Iyengar, S. S.; Tomasi, J.; Barone, V.; Mennucci, B.; Cossi, M.; Scalmani, G.; Rega, N.; Petersson, G. A.; Nakatsuji, H.; Hada, M.; Ehara, M.; Toyota, K.; Fukuda, R.; Hasegawa, J.; Ishida, M.; Nakajima, T.; Honda, Y.; Kitao, O.; Nakai, H.; Klene, M.; Li, X.; Knox, J. E.; Hratchian, H. P.; Cross, J. B.; Bakken, V.; Adamo, C.; Jaramillo, J.; Gomperts, R.; Stratmann, R. E.; Yazyev, O.; Austin, A. J.; Cammi, R.; Pomelli, C.; Ochterski, J. W.; Ayala, P. Y.; Morokuma, K.; Voth, G. A.; Salvador, P.; Dannenberg, J. J.; Zakrzewski, V. G.; Dapprich, S.; Daniels, A. D.; Strain, M. C.; Farkas, O.; Malick, D. K.; Rabuck, A. D.; Raghavachari, K.; Foresman, J. B.; Ortiz, J. V.; Cui, Q.; Baboul, A. G.; Clifford, S.; Cioslowski, J.; Stefanov, B. B.; Liu, G.; Liashenko, A.; Piskorz, P.; Komaromi, I.; Martin, R. L.; Fox, D. J.; Keith, T.; Al-Laham, M. A.; Peng, C. Y.; Nanayakkara, A.; Challacombe, M.; Gill, P. M. W.; Johnson, B.; Chen, W.; Wong, M. W.; Gonzalez, C.; and Pople, J. A. *Gaussian03*; Gaussian, Inc.: Wallingford, CT, 2004.

(20) Ehlers, A. W.; Böhme, M.; Dapprich, S.; Gobbi, A.; Höllwarth, A.; Jonas, V.; Köhler, K. F.; Stegmann, R.; Veldkamp, A.; Frenking, G. *Chem. Phys. Lett.* **1993**, *208*, 111.

(21) Höllwarth, A.; Böhme, M.; Dapprich, S.; Ehlers, A. W.; Gobbi, A.; Jonas, V.; Köhler, K. F.; Stegmann, R.; Veldkamp, A.; Frenking, G. *Chem. Phys. Lett.* **1993**, *208*, 237.

6–31G(d,p)[22] basis sets. The geometry optimizations were performed without any symmetry constraints, and the local minima and the transition states were checked by frequency calculations. For each transition-state structure, the intrinsic reaction coordinate (IRC) routes were calculated in both directions toward the corresponding minima. For some of the transition states, the IRC calculations failed to reach the energy minima on the potential energy surface; therefore, in those cases geometry optimizations were carried out as a continuation of the IRC path. Because of the polarity of the structures, the solvent effects on their relative stabilities were evaluated by calculating the free energies of solvation in terms of the polarizable continuum model (PCM).[23] The self-consistent reaction field (SCRF) calculations using the PCM-UA0 solvation model[24] were carried out for the gas-phase optimized structures as well as the PCM optimized structures. The dielectric constant in the PCM calculations was set to $\varepsilon = 7.58$ to simulate THF as the solvent medium used in the experimental study.[23] The energies discussed throughout the text are both Gibbs free energies in gas phase and total free energies in solution, which have been calculated at 298.15 K and 1 atm.

X-ray Crystal Structure Analyses. For each structure determination, a crystal was placed onto the tip of a 0.1 mm diameter glass fiber and mounted on a Siemens SMART CCD Platform diffractometer for a data collection at 193(2) K.[25] A preliminary set of cell constants and an orientation matrix were calculated from 84 reflections for **3** and 144 reflections for **4** harvested from three sets of 12 frames. These initial sets of frames were oriented such that orthogonal wedges of reciprocal space were surveyed. The data collection was carried out using Mo Kα radiation (graphite monochromator) with a detector distance of 5.09 cm and a frame time of 30 s for **3** and 10 s for **4**. A randomly oriented region of reciprocal space was surveyed to the extent of one sphere and to a resolution of 0.76 Å for **3** and 0.75 Å for **4**. Three major sections of frames were collected with 0.30° steps in ω at three different ϕ settings and a detector position of –28° in 2θ. The intensity data were corrected for absorption.[26] Final cell constants were calculated from the *xyz* centroids of 6497 and 7442 strong reflections for **3** and **4**, respectively, from the actual data collection after integration.[27]

Each structure was solved and refined using SHELXS-97.[28] The space groups $P2_1/n$ for **3** and $P2_12_12_1$ for **4** were determined based on systematic absences and intensity statistics. A direct-methods solution was calculated which provided most nonhydrogen atoms from the E-map. Full-matrix least-squares/difference Fourier cycles were performed which located the remaining nonhydrogen atoms. All nonhydrogen atoms were refined with anisotropic displacement parameters. All hydrogen atoms were placed in ideal positions and refined as riding atoms with relative isotropic displacement parameters. The final full matrix least-squares refinement converged to R_1 values of 0.0569 for **3** and 0.0247 for **4** (F^2, $I > 2\sigma(I)$) and wR_2 values of 0.0978 for **3** and 0.0445 for **4** (F^2, all data). See Supporting Information, Table SI-1 for additional crystal and refinement information.

Acknowledgment. We would like to acknowledge the NSF for financial support (CHE-0414325). We thank Sébastien Lachaize for helpful discussions.

Supporting Information Available: 2D-NMR spectra, crystal and refinement information for **3** and **4**, optimized geometries of the ground-state and transition state structures, as well as the fragments in gas phase, portions of Gaussian input files for the geometry optimizations in gas phase and PCM corrections, experimental and calculated data points used in Figure 5, and simulation regression log file (PDF). This material is available free of charge via the Internet at http://pubs.acs.org.

IC702273A

(22) Hehre, W. J.; Ditchfield, R.; Pople, J. A. *J. Chem. Phys.* **1972**, *56*, 2257.
(23) This model treats the solvent as a sphere of the appropriate size that is rolled over the surface of the molecule, with the dipole of the solvent interacting optimally to stabilize the molecule. See Miertuš, S.; Scrocco, E.; Tomasi, J. *Chem. Phys.* **1981**, *55*, 117.
(24) Barone, V.; Cossi, M.; Tomasi, J. *J. Chem. Phys.* **1997**, *107*, 3210.
(25) *SMART*, V5.629; Bruker Analytical X-ray Systems: Madison, WI, 2003.
(26) SADABS V2.10, An empirical correction for absorption anisotropy, R. Blessing, *Acta Cryst.* **A51**, 33–38 (1995).
(27) *SAINT*, V7.06A; Bruker Analytical X-ray Systems: Madison, WI, 2003.
(28) *SHELXTL*, V6.14; Bruker Analytical X-ray Systems: Madison, WI, 2000.